

Effective source term in the diffusion equation for photon transport in turbid media

Sergio Fantini, Maria Angela Franceschini, and Enrico Gratton

The Green's function for the diffusion equation is widely used to describe photon transport in turbid media. We have performed a series of spectroscopy experiments on a number of uniform turbid media with different optical properties (absorption coefficient in the range $0.03\text{--}0.14\text{ cm}^{-1}$, reduced scattering coefficient in the range $5\text{--}22\text{ cm}^{-1}$). Our experiments have been conducted in the frequency domain, where the measured parameters are the dc intensity (I_{dc}), ac amplitude (I_{ac}), and phase (Φ) of the light intensity wave. In an infinite medium, the Green's function predicts a linear dependence of $\ln(rI_{dc})$ and Φ on the source–detector separation r . Our measurements show that the intercepts of these straight lines predicted by the Green's function do not agree with the experimental results. To reproduce the experimental results, we have introduced an effective photon source whose spatial extent and source strength depend on the optical properties of the medium. This effective source term has no effect on the slopes of the straight lines predicted by the Green's function at large values of r . © 1997 *Optical Society of America*

Key words: Diffusion equation, photon migration, Green's function, frequency domain, turbid media, tissue spectroscopy.

1. Introduction

The properties of light propagation in scattering media are important in many areas of physics and engineering such as remote sensing of the atmosphere,^{1,2} studies of interstellar dust,³ industrial production monitoring,⁴ and medical diagnostics.⁵ The Boltzmann transport equation describes the photon transport in the presence of scattering. In the strongly scattering regime, the Boltzmann transport equation reduces to the diffusion equation, which also describes heat conduction in solids, diffusion of neutrons in condensed media, and gas diffusion. Near-infrared (NIR) light is strongly scattered inside most biological tissues, so the diffusion equation has been widely employed in studies focused on NIR imaging and spectroscopy of living tissue. These applications to medical diagnostics have raised much interest in recent years because of a number of promising preliminary results and because of their significant potential.⁶ Optical measurements in biological tis-

ues can be quantitative. In other words, they can provide absolute values of the optical coefficients that characterize the tissue. These coefficients are the absorption (μ_a) and the reduced scattering (μ_s') coefficients, both in units of inverse centimeters. It has been known for a long time that absorption properties of blood-perfused tissues can be related to hemoglobin content and saturation,⁷ and recent studies have suggested that scattering properties are due to the mitochondrial compartment⁸ and may be related to blood glucose concentration.^{9,10}

To exploit the capability of optical methods to be quantitative, it is necessary to have an accurate expression that describes light propagation in tissues. The common expressions are based on the Green's function for the diffusion equation and thereby assume that the light source is pointlike. The fact that light propagation is not diffusive near the source suggests that, to solve the diffusion equation, one should consider an effective photon source characterized by a spatial extension and a source strength that could depend on the optical properties of the medium. In this work, we have investigated the properties of the effective source (spatial extension and strength) that are consistent with the experimental results. To separate the effects of spatial extension and effective source strength on the detected signal, we have carried out a study in the frequency domain. This approach employs a light source that is intensity

The authors are with the Department of Physics, Laboratory for Fluorescence Dynamics, University of Illinois at Urbana-Champaign, 1110 West Green Street, Urbana, Illinois 61801-3080.

Received 15 April 1996; revised manuscript received 4 September 1996.

0003-6935/97/010156-08\$10.00/0

© 1997 Optical Society of America

modulated at radio frequency (120 MHz in this study). The directly measured parameters are the average intensity (dc) and the amplitude (ac) and phase (Φ) of the light intensity wave. The phase Φ is independent of the source strength, so it can be employed to investigate specifically the spatial extension of the effective photon source. The source strength can then be studied with the dc or ac component of the intensity. In this study, we have considered the phase and the dc intensity, and we have employed optical fibers for both delivering and collecting the optical signal. Our measurements are conducted in a liquid turbid medium with optical properties similar to those of biological tissue in the NIR. In the theory section, Section 2, we also comment on the measurable quantity in our experiment.

2. Theory

A. Measurable Quantity

An optical fiber of numerical aperture N collects photons whose directions of propagation are within the solid angle $2\pi \int_0^{\arcsin N} \sin \theta d\theta$. Within this solid angle, the photon current dI collected in $d\Omega$ around direction $\hat{\Omega}$ by a fiber of area ΔA located at \mathbf{r} is given by

$$dI = vu(\mathbf{r}, t, \hat{\Omega}) \hat{\Omega} \cdot \hat{\mathbf{n}} d\Omega \Delta A, \quad (1)$$

where v is the speed of light in the medium, $u(\mathbf{r}, t, \hat{\Omega})$ is the angular photon density [$hvvu(\mathbf{r}, t, \hat{\Omega})$ is the radiance, where h is Planck's constant and v is the light frequency], and $\hat{\mathbf{n}}$ is the unit vector normal to the surface of the fiber tip and pointing inside the fiber. The total collected current is

$$I = \Delta A 2\pi \int_0^{\arcsin N} vu(\mathbf{r}, t, \hat{\Omega}) \cos \theta \sin \theta d\theta, \quad (2)$$

where the polar axis is in the direction of $\hat{\mathbf{n}}$. If we assume that the presence of the optical fiber does not perturb the angular photon density distribution, Eq. (2) shows that the measurable quantity is the radiance integrated over the solid angle of collection of the fiber. In the diffusion approximation, the radiance is given by the sum of an isotropic term and a smaller directional flux:

$$hvvu(\mathbf{r}, t, \hat{\Omega}) = \frac{hvvU(\mathbf{r}, t)}{4\pi} - \frac{3hvvD}{4\pi} \nabla U \cdot \hat{\Omega}, \quad (3)$$

where $U(\mathbf{r}, t)$ is the photon density [$hvvU(\mathbf{r}, t)$ is the fluence rate], and D is the diffusion coefficient defined as $1/(3\mu_s')$, where μ_s' is the reduced scattering coefficient. If we define $\theta_F = \arcsin N$ ($\theta_F < \pi/2$) to be the acceptance angle of the detector fiber and if $U \propto [\exp(-kr)]/r$, then the photon current collected by a

fiber pointing toward the source ($\hat{\mathbf{n}} = \hat{\mathbf{r}}$) is given by

$$I = \Delta A \frac{vU}{2} \times \left[\frac{1}{4} (1 - \cos 2\theta_F) + D \frac{1+kr}{r} (1 - \cos^3 \theta_F) \right]. \quad (4)$$

The ac amplitude I_{ac} is given by the amplitude of I [and the dc intensity is $I_{dc} = I_{ac}(\omega = 0)$], and the phase Φ is given by the argument of I . In the spherically symmetric case, ∇U is directed along $\hat{\mathbf{r}}$. Consequently, the flux term has its maximum value along $\hat{\mathbf{r}}$, whereas it is 0 in directions perpendicular to $\hat{\mathbf{r}}$. In other words, if the detector fiber points toward the source ($\hat{\mathbf{n}} = \hat{\mathbf{r}}$), the radiance is

$$hvvu(\mathbf{r}, t, \hat{\mathbf{r}}) = \frac{hvvU(\mathbf{r}, t)}{4\pi} - \frac{3hvvD}{4\pi} |\nabla U|, \quad (5)$$

and in directions $\hat{\theta}$ and $\hat{\phi}$ the radiance is

$$hvvu(\mathbf{r}, t, \hat{\theta}) = hvvu(\mathbf{r}, t, \hat{\phi}) = \frac{hvvU(\mathbf{r}, t)}{4\pi} \quad (6)$$

and is proportional to the photon density. Because in the diffusion approximation the directional flux is small compared with the isotropic term, we can conclude that the detected signal is approximately proportional to the photon density $U(\mathbf{r}, t)$ also in the case $\hat{\mathbf{n}} = \hat{\mathbf{r}}$. This discussion is in agreement with Haskell *et al.*,¹¹ although it deviates from the conclusions of other authors who consider the photon flux ($-vD\nabla U \cdot \hat{\mathbf{n}}$) (Ref. 12) or the photon current density¹³ to be the measurable quantity. The photon flux describes the net flow of photons through a given surface, but an optical fiber is sensitive only to a part of the solid angle, i.e., to a partial current. Liu *et al.*¹⁴ have also experimentally shown that for the case $\hat{\mathbf{n}} = \hat{\theta}$, the measured quantity is proportional to the photon density rather than to the photon flux. As a conclusive remark, we also note that in the case $\hat{\mathbf{n}} = \hat{\theta}$ the photon flux is 0, whereas the experimentally measured signal is comparable with that measured in the case $\hat{\mathbf{n}} = \hat{\mathbf{r}}$.

B. Diffusion Equation

The diffusion equation for photon transport in a macroscopically homogeneous turbid medium is¹⁵

$$\frac{\partial U(\mathbf{r}, t)}{\partial t} - vD\nabla^2 U(\mathbf{r}, t) + v\mu_a U(\mathbf{r}, t) = q(\mathbf{r}, t), \quad (7)$$

where $q(\mathbf{r}, t)$ is the source term. The frequency-domain Green's function for an infinite medium is given by¹⁶

$$U_G(r, \omega) = \frac{1}{4\pi vD} \frac{\exp(-kr)}{r}, \quad (8)$$

where $k^2 = (v\mu_a - i\omega)/(vD)$ and ω is the angular modulation frequency of the source intensity.

C. Spatially Extended Photon Source

The solution to the diffusion equation [Eq. (7)] for a spatially extended photon source, described by the source term $q(\mathbf{r})$, is given by the convolution between $q(\mathbf{r})$ and the Green's function:

$$U(\mathbf{r}, \omega) = q(\mathbf{r}) * U_G(r, \omega) = \int q(\mathbf{r}') U_G(|\mathbf{r} - \mathbf{r}'|, \omega) d^3\mathbf{r}'. \quad (9)$$

In spherical coordinates, with the polar axis along \mathbf{r} , the convolution integral becomes

$$q(\mathbf{r}) * U_G(r, \omega) = \int_0^{2\pi} d\phi' \int_0^\pi d\theta' \sin \theta' \int_0^\infty dr' r'^2 q(r', \theta', \phi') \frac{1}{4\pi\nu D} \frac{\exp[-k(r^2 + r'^2 - 2rr' \cos \theta')^{1/2}]}{(r^2 + r'^2 - 2rr' \cos \theta')^{1/2}}. \quad (10)$$

The photon densities for a number of spherically symmetric photon sources $q(r)$ are reported in Appendix 1.

The anisotropic emission of an optical fiber with a large numerical aperture (~ 1) can be modeled by an effective photon source spatially distributed within a hemisphere of radius γ centered at the fiber tip. In this way, we account for the directional emission in half of the solid angle (see Fig. 1). The scattering centers inside the medium act as effectively isotropic point sources, as has already been suggested,¹⁷ so that we can apply Eq. (10) to find $U_{\text{hs}}(r, \omega)$ (where the subscript hs stands for hemisphere). The source term $q(r', \theta', \phi')$ is written as

$$q(r', \theta', \phi') = \begin{cases} 3S_{\text{eff}}(\omega)/2\pi\gamma^3, & \text{for } 0 \leq r' \leq \gamma \text{ and } 0 \leq \theta' \leq \pi/2 \\ 0, & \text{for } r' > \gamma \text{ or } \pi/2 < \theta' \leq \pi \end{cases}, \quad (11)$$

where $S_{\text{eff}}(\omega)$ is the total effective source strength, i.e., the number of photons per unit time emitted in the whole volume of the hemisphere. The result for $U_{\text{hs}}(r, \omega)$ at $r > \gamma$ and $\theta = 0$ (i.e., along the fiber axis) obtained by the computation of the integral in Eq. (10) is

$$U_{\text{hs}}(r, \omega) = S_{\text{eff}}(\omega) U_G(r, \omega) \frac{3}{k^3 \gamma^3} \times \left(\left[1 + kr \left(1 + \frac{\gamma^2}{r^2} \right)^{1/2} \right] \exp \left\{ kr \left[1 - \left(1 + \frac{\gamma^2}{r^2} \right)^{1/2} \right] \right\} - kr + (k\gamma - 1) \exp(k\gamma) \right). \quad (12)$$

We note that in the limit $\gamma \rightarrow 0$, $U_{\text{hs}}(r, \omega)$ reduces to $S_{\text{eff}}(\omega) U_G(r, \omega)$ as it should. It is also noteworthy that in the limit $r \rightarrow \infty$, or $r^2 \gg \gamma^2$, $U_{\text{hs}}(r, \omega)$ becomes proportional to $U_G(r, \omega)$ with a constant of proportionality independent of r . The r dependence of



Fig. 1. Source fiber that delivers the light to the sample and the detector fiber that collects the optical signal. The effective photon source is distributed in a hemisphere (shaded) centered at the tip of the source fiber and has a radius γ .

$U_{\text{hs}}(r, \omega)$ at $r^2 \gg \gamma^2$ is thus the same as that of the Green's function, i.e., $\exp(-kr)/r$.

3. Experimental Methods

A. Strongly Scattering Material

The strongly scattering material employed in our study is a 9-L liquid suspension containing water, Liposyn 20%, and black India ink. Liposyn is a fat emulsion that acts as a weak absorber and a strong scatterer for NIR light. The reduced scattering coefficient of the medium is proportional to the concentration (v/v) of Liposyn, where the proportionality factor is $\sim 2.2 \text{ cm}^{-1}/\%$ (v/v) [or, in terms of percentage of solids content (s.c.), $\sim 11 \text{ cm}^{-1}/\%$ (s.c.)]. In our study, we have investigated reduced scattering coefficients ranging from 5 to 22 cm^{-1} (with $\mu_a = 0.035 \text{ cm}^{-1}$). Black India ink is employed to vary the absorption coefficient in the range 0.035–0.14 cm^{-1} (with $\mu_s' = 16 \text{ cm}^{-1}$). The 9-L strongly scattering suspension is placed in a rectangular container of sides 32 cm \times 26 cm \times 12 cm.

B. Frequency-Domain Spectrometer

The light source is a laser diode emitting at 780 nm (Sharp LT023). Its output, which is amplitude modulated at a frequency of 120 MHz, is coupled to a plastic optical fiber with a core diameter of 2 mm and a numerical aperture of 0.5 ($\theta_F = 30^\circ$). Intensity modulation of the laser diode is accomplished by supplying a dc current of 50 mA (which selects a working point just above threshold) and a superimposed 120-MHz oscillating signal. As a result, the average emitted power is $\sim 3 \text{ mW}$ and the modulation depth is close to 100%. The radio frequency signal is provided by a frequency synthesizer (Marconi 2022A) that is phase locked to a second frequency synthesizer (Marconi 2022A). This latter synthesizer modulates the gain of the photomultiplier tube (PMT) detector (Hamamatsu R928) at a frequency of 120 MHz + 400 Hz. The signals from both frequency synthesizers are amplified by radio frequency amplifiers (ENI Model 403LA). The beating between the detected signal at 120 MHz and the response function

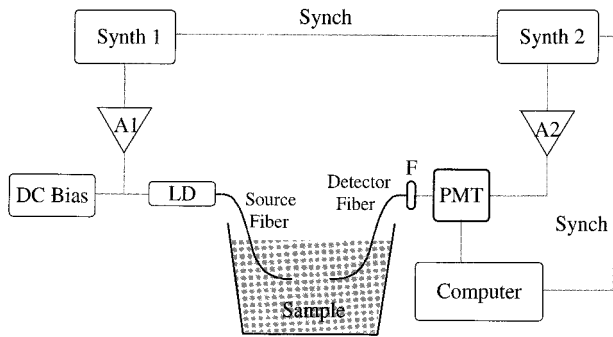


Fig. 2. Experimental arrangement. The laser diode (LD) emitting at 780 nm is intensity modulated at 120 MHz by a frequency synthesizer (Synth 1) by means of amplifier A1. The DC Bias selects a working point for the laser diode just above threshold. The tips of the source and the detector optical fibers are immersed in the sample to mimic an infinite geometry. The two fibers face each other, and the volume of the sample is ~ 9 L. The gain of the PMT detector is modulated at 120 MHz + 400 Hz by synthesizer 2 (Synth 2) by means of amplifier A2. Neutral-density filters (F) are used to attenuate the detected signal at smaller source–detector separations. The data acquisition card in the computer and the two frequency synthesizers are phase locked (Synch).

of the PMT at 120 MHz + 400 Hz gives rise to a harmonic component at 400 Hz in the PMT output signal. This low-frequency component is processed to yield the frequency-domain parameters dc (average intensity), ac (amplitude of the intensity wave), and Φ (phase of the intensity wave) by the use of previously described methods.¹⁸

C. Measurement Procedure

The experimental arrangement is shown in Fig. 2. The tips of the source and the detector fibers are placed deep in the suspension such that we work in an effective infinite geometry. The two fibers face each other as shown in Fig. 1. We used two identical 9-L containers, one for media of different absorption coefficients, and one for media of different reduced scattering coefficients. We investigated seven media with μ_a ranging from 0.035 to 0.14 cm^{-1} (and with $\mu_s' = 16 \text{ cm}^{-1}$) and five media with μ_s' ranging from 5 to 22 cm^{-1} (and with $\mu_a = 0.035 \text{ cm}^{-1}$). For each medium we measured the intensity signal at source–detector separations ranging from 0 (fiber tips in contact) to 2 cm, at 0.1-cm increments. To perform the measurement in the required intensity dynamic range ($\sim 10^5$), we employed neutral density filters at the PMT detector (whose high voltage supply was kept constant throughout the experiment).

4. Results

A. Determination of μ_a and μ_s'

In a previous publication,¹⁹ we proposed a multidistance measurement protocol for the absolute determination of μ_a and μ_s' in optically dense media. This protocol consists of acquiring data at a number (at least two) of different source–detector separations, from which one can determine the slopes of the

straight lines $\ln(rI_{dc})$, $\ln(rI_{ac})$, and Φ as a function of r . The Green's function of Eq. (8) provides expressions for these slopes that enable one to calculate μ_a and μ_s' . As we comment in Appendix 1, a spherically symmetric light source that is confined at $r \leq \gamma$ does not change the expressions for these slopes at $r > \gamma$. The spherically asymmetric source distribution of Eq. (11) also does not change the expression for these slopes at $r^2 \gg \gamma^2$. An important consequence is that a measurement of μ_a and μ_s' based on the slopes of $\ln(rI_{dc})$, $\ln(rI_{ac})$, and Φ at large r is not affected by the details of the source spatial distribution. We have thus determined μ_a and μ_s' of our media by applying the multidistance measurement protocol to the data collected at r between 1.5 and 2.0 cm.

B. Spatial Extension of the Effective Photon Source

Because the slopes of the straight lines discussed in Section 3 are not affected by the source spatial distribution and by the source strength, we have focused our attention on the intercepts. In particular, the phase intercept is not affected by the source strength, so that the phase intercept data give information specifically on the source spatial extent. Figure 3 shows the experimental phase intercepts as a function of μ_a [Fig. 3(a)] and μ_s' [Fig. 3(b)]. We observe that the phases are relative to the phase measured at $r = 0$, i.e., with the source and the detector fiber tips in contact. For comparison, we also report the phase intercept predicted by the integrated radiance [Eq. (4)] calculated with $\theta_F = 30^\circ$ by using $U_G(r, \omega)$ [Eq. (8)] and $U_{hs}(r, \omega)$ [Eq. (12)]. In $U_{hs}(r, \omega)$ we set

$$\gamma = \frac{1}{\text{Re}[k(\mu_a, \mu_{s0}')]}, \quad (13)$$

$$= \frac{1}{\left(\frac{3}{2} \mu_a \mu_{s0}'\right)^{1/2} \left[\left(1 + \frac{\omega^2}{v^2 \mu_a^2}\right)^{1/2} + 1 \right]^{1/2}},$$

where $\mu_{s0}' = 16 \text{ cm}^{-1}$ is a constant. This value of γ , which reduces to $1/(3\mu_a \mu_{s0}')^{1/2}$ for the dc intensity, is of the order of the diffusion length and ranges from 0.4 to 0.8 cm for the media considered in this study. The diffusion length characterizes the spatial scale of the photon density decay. It also gives an estimate of the distance from the actual source over which the diffusive regime is established. This distance is larger than the photon mean free path between effectively isotropic scattering events, which is given by $1/\mu_s'$. We note here that γ , the extension of the effective source, is a function of μ_a and ω , but surprisingly not of μ_s' [μ_{s0}' in Eq. (13) is a constant]. The constant value of $\mu_{s0}' = 16 \text{ cm}^{-1}$ used in Eq. (13) provides a good agreement between our model and experiment, even in the case of media that have different values of μ_s' [see Fig. 3(b)]. We also observe that $U_{hs}(r, \omega)$ with γ given by Eq. (13) accurately describes not only the dependence of the experimental phase intercept on μ_a and μ_s' , but also its absolute value.

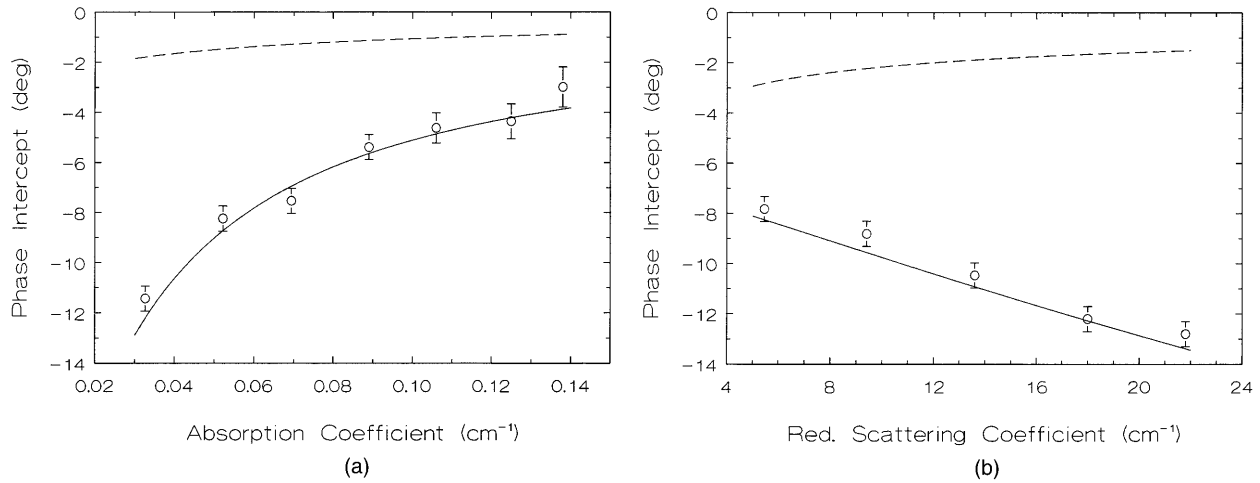


Fig. 3. Intercept of the phase-versus- r straight line as a function of (a) μ_a , (b) μ_s' . In (a), μ_s' is 16 cm^{-1} , whereas in (b), μ_a is 0.035 cm^{-1} . The symbols are the experimental values obtained from the phase data taken at r ranging between 1.5 and 2 cm. The curves are the phase intercepts predicted by diffusion theory for a point source (dashed curve) and for the effective extended source described in the text (solid curve).

C. Source Strength of the Effective Photon Source

Once the effective source extension has been determined by Eq. (13), the intercepts of the intensity straight lines provide information on the effective source strength. Figure 4 shows the experimental intercepts of $\ln(rI_{dc})$ as a function of μ_a [Fig. 4(a)] and μ_s' [Fig. 4(b)]. For comparison, we also show the intercepts predicted by the integrated radiance [Eq. (4)] calculated with $\theta_F = 30^\circ$ by using $U_G(r, \omega)$ [Eq. (8)] and $U_{hs}(r, \omega)$ [Eq. (12)]. In $U_{hs}(r, \omega)$ we have used the expression of Eq. (13) for γ and we have set

$$S_{\text{eff}} \propto S \frac{\mu_a}{\mu_s'}, \quad (14)$$

where S is the actual source strength. This effective source strength is compatible with our experimental

results for the intensity intercepts (see Fig. 4). In contrast to the phase intercepts, the absolute values of the experimental and the predicted intensity intercepts cannot be compared because of the unknown effect of the instrumental response. For this reason, the predicted intensity intercepts in Fig. 4 are shifted by an arbitrary offset. The fact that S_{eff} decreases with μ_s' is reasonable. In fact, the source dimension γ does not change with μ_s' , and the number of photons emitted per unit time by the effective source is reduced by the scattering-induced absorption. The increase of S_{eff} with μ_a is apparently surprising. It is the net result of two competing effects determined by an increase in the absorption coefficient. The first effect is the reduction in the number of photons emitted per unit time by the effective source because of the increased absorption. The second effect is the

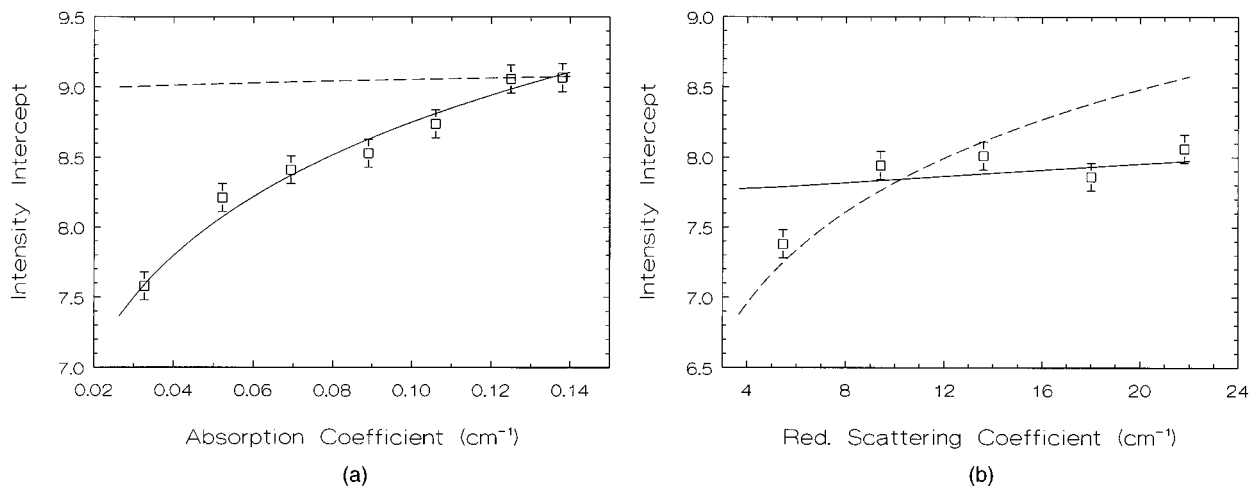


Fig. 4. Intercept of the $\ln(rI_{dc})$ -versus- r straight line as a function of (a) μ_a , (b) μ_s' . In (a), μ_s' is 16 cm^{-1} , whereas in (b), μ_a is 0.035 cm^{-1} . The symbols are the experimental values obtained from the intensity data taken at r ranging between 1.5 and 2 cm. The curves are the intensity intercepts predicted by diffusion theory for a point source (dashed curve) and for the effective extended source described in the text (solid curve).

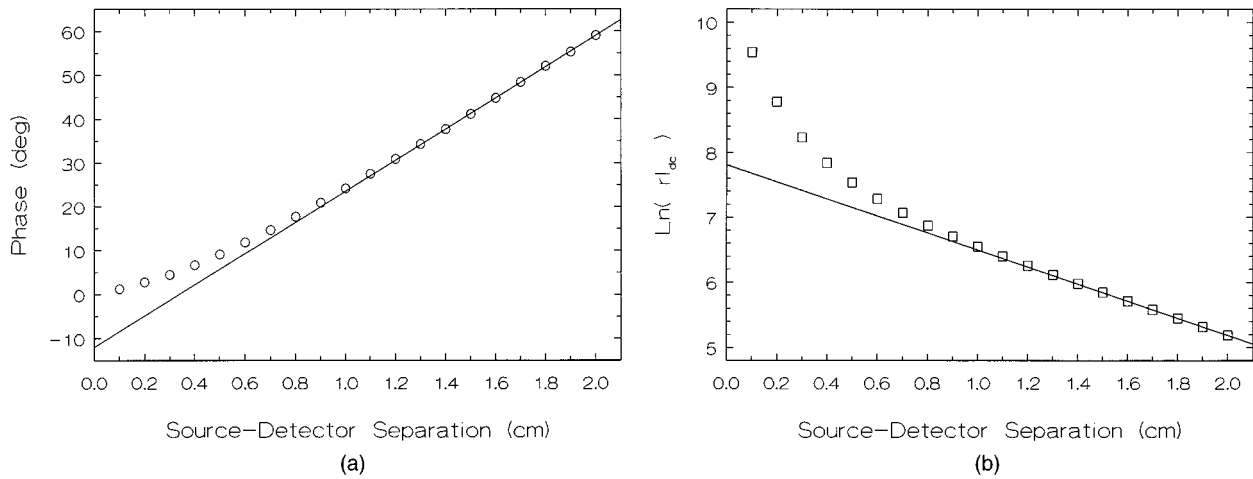


Fig. 5. Symbols represent (a) the measured phase, (b) $\ln(rI_{dc})$ as functions of source-detector separation r . The medium has an absorption coefficient of $\mu_a = 0.035 \text{ cm}^{-1}$ and a reduced scattering coefficient of $\mu_s' = 18 \text{ cm}^{-1}$. Consequently the radius of the hemispheric effective photon source is $\gamma = 0.71 \text{ cm}$. The continuous curves have the slopes predicted by diffusion theory and are shifted by an offset to match the experimental data at $r > \gamma$. At $r < \gamma$ the experimental points deviate significantly from the linear behavior predicted by diffusion theory.

reduction in the source dimensions ($\gamma \propto 1/\sqrt{\mu_a}$), which confines the effective source volume closer to the actual photon source. This second effect reduces the probability of photon absorption within the effective source volume.

The inclusion of the following effects, (1) integrated radiance over the acceptance angle ($< \pi/2$) of the optical fiber, (2) hemispheric light source with radius γ given by Eq. (13), and (3) effective source strength given by Eq. (14), results in the following expression for the experimentally measured intensity at large r ($r \gg \gamma$) and $\theta = 0$:

$$I(r, \omega) \propto S\Delta A \frac{\mu_a}{k^3 \gamma^3} [1 + (k\gamma - 1)\exp(k\gamma)] \times \left[\frac{1}{4} (1 - \cos 2\theta_F) + Dk(1 - \cos^3 \theta_F) \right] \frac{\exp(-kr)}{r}. \quad (15)$$

5. Discussion and Conclusion

The experimental results shown in Figs. 3 and 4 show the inadequacy of the diffusion-equation Green's function in describing the dependence of the intercepts of dc intensity and phase on μ_a and μ_s' . Such inadequacy cannot be resolved by modeling the light source (a 2-mm-diameter optical fiber in our case) with an extended photon source of given dimensions. On the contrary, the experimental results can be reproduced by assuming that there is an effective photon source whose spatial extent and strength depend on μ_a and μ_s' . We have found that the dimensions of the effective photon source γ is of the order of the diffusion length, which represents the distance over which the photon migration becomes diffusive. Figure 5 shows the different r dependencies of the experimental data at $r < \gamma$ and $r > \gamma$ for the case $\mu_a = 0.035 \text{ cm}^{-1}$ and $\mu_s' = 18 \text{ cm}^{-1}$. In this case, the

effective source dimension γ is 0.71 cm. Because the diffusion-equation Green's function is accurate only at $r > \gamma$, the different regime at $r < \gamma$ explains the failure of the Green's function in predicting the dc and phase intercepts. This observation has important consequences in quantitative spectroscopy of turbid media. The measurement of the slopes of the dc and phase straight lines versus r provides accurate values of μ_a and μ_s' (Ref. 19). However, to measure these slopes, one needs to acquire data at multiple source-detector separations at which different volumes are sampled by the photon paths. In applications in which the sample is not macroscopically homogeneous, this fact can represent a problem. Consequently algorithms that employ a calibration measurement followed by one measurement at a single source-detector separation have been proposed.²⁰ A similar algorithm has been proposed in steady-state spectroscopy,²¹ in which the slope and intercept of the dc straight line are used to determine μ_a and μ_s' . These algorithms are based on the diffusion-equation Green's function and employ the intercepts as well as the slopes of the straight lines associated with the measured quantities. As a result of this study, these algorithms are not expected to provide accurate results, unless the calibration medium and the sample have the same optical properties.

The properties of the effective photon source (γ and S_{eff}) have been empirically derived here to provide an accurate description of our experimental results. However, we have not developed a model starting from first principles, which explains the physical origin of the discrepancy between the experimental data and the predictions of diffusion theory. It is possible that the acquisition geometry (relative orientation of the source and the detector fibers) and the numerical apertures of the optical fibers play a role in our observations that has not been quantified. How-

ever, the effects that we observed are so large that they cannot be ignored. Other researchers have observed similar effects (nonzero phase intercepts in a plot of phase versus source–detector separation) in a geometry in which the source and detector fibers were not facing each other.¹¹ Their phase intercepts at 100 MHz were larger than +10°, and this result could not be explained.

In conclusion, this work points out an important limitation of the Green's function solution (i.e., the solution for a point-like source) to the diffusion equation for measurements of photon transport in turbid media. More work is required for investigating the physical origin of this limitation and to assess the influence of the specific source–detector configuration used to measure the optical parameters of a turbid medium.

Appendix A: Photon Densities for Some Spherically Symmetric Photon Sources

In this Appendix, we consider four spherically symmetric photon sources described by $q(r)$. We indicate the source strength at angular frequency ω with $S(\omega)$ and the linear dimension of the source with γ . For each of these source terms, we have derived the photon density in the diffusion regime by applying Eq. (10).

1. Spherical Source with Constant Strength

The source term for a constant photon source in the sphere of radius γ is

$$q_{\Pi}(r) = \frac{3S(\omega)}{4\pi\gamma^3} \Pi(r/\gamma), \quad (\text{A1})$$

where $\Pi(r/\gamma)$ is defined to be 1 if $r \leq \gamma$ and 0 if $r > \gamma$. The resultant photon density at $r > \gamma$ is

$$U_{\Pi}(r, \omega) = SU_G(r, \omega) \frac{3}{k^3\gamma^3} [k\gamma \cosh(k\gamma) - \sinh(k\gamma)], \quad (\text{A2})$$

where $k^2 = (v\mu_a - i\omega)/(vD)$ and $U_G(r, \omega)$ is given by Eq. (8).

2. Spherical Source with a Strength Linearly Decreasing from the Center

The source term for a spherical photon source with radius γ and with a strength that decreases linearly with distance from the center is

$$q_{\Lambda}(r) = \frac{3S(\omega)}{\pi\gamma^3} \Lambda(r/\gamma), \quad (\text{A3})$$

where $\Lambda(r/\gamma)$ is defined to be $1 - r/\gamma$ if $r \leq \gamma$ and 0 if $r > \gamma$. The resultant photon density at $r > \gamma$ is

$$U_{\Lambda}(r, \omega) = SU_G(r, \omega) \frac{12}{k^4\gamma^4} [k\gamma \sinh(k\gamma) - 2 \cosh(k\gamma) + 2]. \quad (\text{A4})$$

3. Distributed Source with a Strength Decreasing Stronger than Exponentially from the Center

The source term for a spherically symmetric source whose strength decreases with r like the diffusion-equation Green's function is

$$q_{\text{exp}}(r) = \frac{S(\omega)}{4\pi\gamma^2} \frac{\exp(-r/\gamma)}{r}. \quad (\text{A5})$$

This source term represents an indefinitely distributed source with a source strength decaying with r as $\exp(-r/\gamma)/r$. The characteristic decay length of this source is γ , and the characteristic decay length of the Greens' function [Eq. (8)] is $1/\text{Re}(k)$. The photon density that corresponds to this source term is

$$U_{\text{exp}}(r, \omega) = SU_G(r, \omega) \frac{\exp\left[-(1 - k\gamma) \frac{r}{\gamma}\right]}{1 - k^2\gamma^2}. \quad (\text{A6})$$

4. Spherical Shell

The source term for a spherical shell of radius γ is

$$q_{\text{shell}}(r) = \frac{S(\omega)}{4\pi\gamma^2} \delta(r - \gamma), \quad (\text{A7})$$

where $\delta(r - \gamma)$ is the Dirac delta. The corresponding photon density at $r > \gamma$ is

$$U_{\text{shell}}(r, \omega) = SU_G(r, \omega) \frac{\sinh(k\gamma)}{k\gamma}. \quad (\text{A8})$$

We observe that in the limit $\gamma \rightarrow 0$, all four source distributions 1-4 become a photon point source. In this limit, as expected, we have

$$\lim_{\gamma \rightarrow 0} U_{\Pi} = \lim_{\gamma \rightarrow 0} U_{\Lambda} = \lim_{\gamma \rightarrow 0} U_{\text{exp}} = \lim_{\gamma \rightarrow 0} U_{\text{shell}} = S(\omega)U_G(r, \omega). \quad (\text{A9})$$

We also note that at distances larger than the effective source extent (i.e., at $r > \gamma$ for sources 1, 2, and 4) the r dependence of the photon density is $\exp(-kr)/r$. This result holds also for source 3, provided that $1/\text{Re}(k) \gg \gamma$. This result indicates that for spherically symmetric sources, the slopes of the straight lines $\ln(rI_{\text{dc}})$, $\ln(rI_{\text{ac}})$, and Φ as a function of r are not influenced by the details of the source spatial distribution.

This work was conducted at the Laboratory for Fluorescence Dynamics, which is supported by the U.S. National Institutes of Health, grant RR03155 and by the University of Illinois at Urbana-Champaign. This research is also supported by U.S. Institutes of Health grant CA57032. We thank Albert Cerussi for providing the fiber-coupled, intensity-modulated laser diode.

References

1. MUSCLE4, Fourth International Workshop on Multiple Scattering Lidar Experiments, Florence, Italy, 29–31 October 1990.
2. J. A. Weinman, "Effects of multiple scattering on light pulses reflected by turbid atmosphere," *J. Atmos. Sci.* **33**, 1763–1771 (1976).
3. B. D. Savage and J. S. Mathis, "Observed properties of interstellar dust," *Ann. Rev. Astron. Astrophys.* **17**, 73–111 (1979).
4. R. R. Alfano, X. Liang, L. Wang, and P. P. Ho, "Time-resolved imaging of oil droplets in highly scattering soil solution," in *Optical Tomography, Photon Migration, and Spectroscopy of Tissue and Model Media: Theory, Human Studies, and Instrumentation*, B. Chance and R. R. Alfano, eds., Proc. SPIE **2389**, 2–5 (1995).
5. G. J. Müller, ed., *Medical Optical Tomography: Functional Imaging and Monitoring*, Vol. IS11 of SPIE Institute Series (Society of Photo-Optical Instrumentation Engineers, Bellingham, Wash., 1993).
6. B. Chance and R. R. Alfano, eds., *Optical Tomography, Photon Migration, and Spectroscopy of Tissue and Model Media: Theory, Human Studies, and Instrumentation*, Proc. SPIE **2389** (1995).
7. G. A. Millikan, "The oximeter, an instrument for measuring continuously the oxygen saturation of arterial blood in man," *Rev. Sci. Instrum.* **13**, 434–444 (1942).
8. B. Beauvoit, T. Kitai, and B. Chance, "Contribution of the mitochondrial compartment to the optical properties of the rat liver: a theoretical and practical approach," *Biophys. J.* **67**, 2501–2510 (1994).
9. M. Kohl, M. Cope, M. Essenpreis, and D. Böcker, "Influence of glucose concentration on light scattering in tissue-simulating phantoms," *Opt. Lett.* **19**, 2170–2172 (1994).
10. J. S. Maier, S. A. Walker, S. Fantini, M. A. Franceschini, and E. Gratton, "Possible correlation between blood glucose concentration and the reduced scattering coefficient of tissues in the near infrared," *Opt. Lett.* **19**, 2062–2064 (1994).
11. R. C. Haskell, L. O. Svaasand, T. T. Tsay, T. C. Feng, M. S. McAdams, and B. J. Tromberg, "Boundary conditions for the diffusion equation in radiative transfer," *J. Opt. Soc. Am. A* **11**, 2727–2741 (1994).
12. S. R. Arridge, M. Cope, and D. T. Delpy, "The theoretical basis for the determination of optical pathlengths in tissue: temporal and frequency analysis," *Phys. Med. Biol.* **37**, 1531–1560 (1992).
13. J.-M. Kaltenbach and M. Kaschke, "Frequency- and time-domain modelling of light transport in random media," in Ref. 5, pp. 65–86.
14. F. Liu, K. M. Yoo, and R. R. Alfano, "Should the photon flux or the photon density be used to describe the temporal profiles of scattered ultrashort laser pulses in random media?," *Opt. Lett.* **18**, 432–434 (1993).
15. J. J. Duderstadt and L. J. Hamilton, *Nuclear Reactor Analysis* (Wiley, New York, 1976), p. 137.
16. J. B. Fishkin and E. Gratton, "Propagation of photon-density waves in strongly scattering media containing an absorbing semi-infinite plane bounded by a straight edge," *J. Opt. Soc. Am. A* **10**, 127–140 (1993).
17. T. J. Farrel, M. S. Patterson, and B. Wilson, "A diffusion theory model of spatially resolved, steady-state diffuse reflectance for the noninvasive determination of tissue optical properties *in vivo*," *Med. Phys.* **19**, 879–888 (1992).
18. B. A. Feddersen, D. W. Piston, and E. Gratton, "Digital parallel acquisition in frequency domain fluorometry," *Rev. Sci. Instrum.* **60**, 2929–2936 (1989).
19. S. Fantini, M. A. Franceschini, J. B. Fishkin, B. Barbieri, and E. Gratton, "Quantitative determination of the absorption spectra of chromophores in strongly scattering media: a light-emitting-diode-based technique," *Appl. Opt.* **33**, 5204–5213 (1994).
20. M. A. Franceschini, S. Fantini, S. A. Walker, J. S. Maier, W. W. Mantulin and E. Gratton, "Multi-channel optical instrument for near-infrared imaging of tissue," in Ref. 6, pp. 264–273.
21. H. Liu, D. A. Boas, Y. Zhang, A. G. Yodh, and B. Chance, "A simplified approach to characterize optical properties and blood oxygenation in tissue using continuous near infrared light," in Ref. 6, pp. 496–502.